

Lattice Boltzmann model for complex Ginzburg–Landau equation in curvilinear coordinates[☆]



Jianying Zhang ^{a,*}, Guangwu Yan ^b

^a School of Basic Sciences, Changchun University of Technology, Changchun, 130012, PR China

^b College of Mathematics, Jilin University, Changchun, 130012, PR China

ARTICLE INFO

Article history:

Received 1 December 2014

Received in revised form 20 August 2015

Accepted 4 October 2015

Available online 1 November 2015

Keywords:

Lattice Boltzmann model

Complex Ginzburg–Landau equation

Spiral wave

Curvilinear coordinates

ABSTRACT

A lattice Boltzmann model is proposed for solving the complex Ginzburg–Landau equation (CGLE) with curvilinear coordinates. The method maintains the algorithmic simplicity of the original lattice Boltzmann scheme, and does not require an interpolation or coarse-graining procedure. This lattice Boltzmann scheme is based on uniformly distributed lattice points in these curvilinear coordinate systems. The algorithm provides advantages similar to the previous lattice Boltzmann method in that it is easily adapted to CGLE. The numerical simulations show spiral wave on a disc, the surface of a sphere, and the inside of a sphere. Examples show that the model accurately reproduces the phenomena in the CGLE.

© 2015 Elsevier Ltd. All rights reserved.

1. Introduction

The LBM has shown a promise for hydrodynamics and other fluid systems [1–3]. However, recent interest in lattice Boltzmann method (LBM) for complex partial differential equations has been motivated by the need of efficient techniques for examining a wide range of difficult nonlinear problems. Some LBM models have been proposed for solving such equations [4–6]. Furthermore, two and three-dimensional complex Ginzburg–Landau equation (CGLE) have been studied and simulated in detail [7]. In addition, the LBM for the complex reaction–diffusion equation (CRDE) was also proposed [8]. These CRDEs describe a number of bimolecular autocatalytic reaction–diffusion systems.

However, the LBM has encountered a challenge from its birth day, namely, how to model LBM in non-Cartesian coordinates. Some researchers have made attempts in this respect, but these schemes require interpolation and coarse techniques [9,10]. A recent development of LBM in the non-Cartesian coordinate system does not require interpolation and coarse treatment, but some of the advantages of LBM were lost [11].

In this paper, we will construct a lattice Boltzmann model in the curvilinear coordinates, including polar coordinates and spherical coordinates. In view of the growing interest in studying the pattern of spiral waves, we give the detailed description of the LBM model in curvilinear coordinates by considering the complex Ginzburg–Landau equation. We argue that this LBM has the same advantages as previous LBMs [7] for complex Ginzburg–Landau equation, and demonstrates through numerical simulations that the model accurately reproduces spiral waves.

[☆] This work is in part supported by the National Natural Science Foundation of China (Grant no. 11272133), and the China Postdoctoral Science Foundation (No. 2011M500002).

* Corresponding author.

E-mail address: zhangjy_ccut@126.com (J. Zhang).

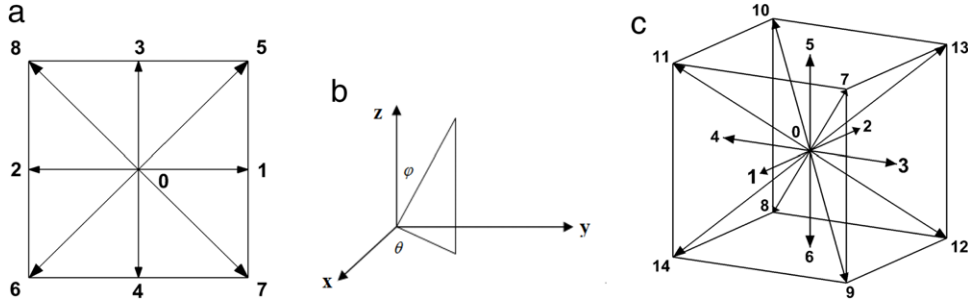


Fig. 1. Diagrammatic sketches: (a) D2Q9 lattice, (b) spherical coordinate, (c) D3Q15 lattice.

The CGLE is the form as following

$$\frac{\partial A}{\partial t} = \beta \nabla^2 A + H(A), \quad (1)$$

where ∇^2 is Laplacian operator, β is a complex diffusion coefficient, $H(A) = aA - d|A|^2A$ is complex function of variable A .

The complex Ginzburg–Landau equations (CGLE) have drawn a great deal of attention in physics and applied mathematics communities as a class of universal models with a broad spectrum of applications, ranging from nonlinear optics, fluid dynamics, and chemical waves to second-order phase transitions, including such topics of common interest as superfluidity, superconductivity, liquid crystals, and Bose–Einstein condensates etc.

The paper is organized as follows: in the next section, the lattice Boltzmann models in the polar coordinates and spherical coordinates for the CGLE are given. In Section 3, numerical simulations for the pattern formation of the CGLE are presented. And in Section 4, some conclusions are discussed.

2. Lattice Boltzmann model for complex Ginzburg–Landau equation in curvilinear coordinates

2.1. CGLE in the polar coordinates

In the two dimensional (2D) space, let us consider the polar coordinate system (r, θ) . We make the coordinate transformation from Cartesian coordinates, which are $x = r \cos \theta$, $y = r \sin \theta$, $0 \leq \theta \leq 2\pi$. In the polar coordinates, Eq. (1) becomes

$$\frac{\partial A}{\partial t} = \beta \left[\frac{\partial^2 A}{\partial r^2} + \frac{\partial^2}{\partial \theta^2} \left(\frac{A}{r^2} \right) \right] + \beta \frac{1}{r} \frac{\partial A}{\partial r} + H(A). \quad (2)$$

To construct the LBM, we set the source term as

$$S(A) = \beta \frac{1}{r} \frac{\partial A}{\partial r} + H(A). \quad (3)$$

2.2. CGLE in the surface of spherical coordinates

We employ a spherical coordinate system (r, φ, θ) , see Fig. 1(b). The spherical coordinates translate into the Cartesian coordinates by $x = r \sin \varphi \cos \theta$, $y = r \sin \varphi \sin \theta$, $z = r \cos \varphi$, $(0 < \varphi < \pi, 0 \leq \theta \leq 2\pi)$.

On the surface of a sphere, the radius of the sphere $r = R$ is a constant. Eq. (1) becomes

$$\frac{\partial A}{\partial t} = \beta \frac{1}{R^2} \left[\frac{1}{\sin \varphi} \frac{\partial}{\partial \varphi} \left(\sin \varphi \frac{\partial A}{\partial \varphi} \right) + \frac{1}{\sin^2 \varphi} \frac{\partial^2 A}{\partial \theta^2} \right] + H(A). \quad (4)$$

To construct the LBM, this equation translates into

$$\frac{\partial A}{\partial t} = \beta \frac{1}{R^2} \left[\frac{\partial^2 A}{\partial \varphi^2} + \frac{\partial^2}{\partial \theta^2} \left(\frac{A}{\sin^2 \varphi} \right) + \frac{\partial(\operatorname{ctg} \varphi A)}{\partial \varphi} + A \csc^2 \varphi \right] + H(A). \quad (5)$$

In Eq. (5), $\beta \frac{A \csc^2 \varphi}{R^2}$ is a source term, $\beta \frac{1}{R^2} \frac{\partial(\operatorname{ctg} \varphi A)}{\partial \varphi}$ is a flux term. How to deal with the flux term $\beta \frac{1}{R^2} \frac{\partial(\operatorname{ctg} \varphi A)}{\partial \varphi}$ is the key step. In fact, this is a “pseudo-convection” term, originated from spherical coordinate’s curvature. Its real identity should be a part of the source terms. In the actual calculation, we deal it with the central difference. Hence, Eq. (5) becomes into

$$\frac{\partial A}{\partial t} = \beta \frac{1}{R^2} \left[\frac{\partial^2 A}{\partial \varphi^2} + \frac{\partial^2}{\partial \theta^2} \left(\frac{A}{\sin^2 \varphi} \right) \right] + S(A), \quad (6)$$

where the source term is

$$S(A) = \beta \frac{1}{R^2} \left[\frac{\partial(\operatorname{ctg}\varphi A)}{\partial\varphi} + A \csc^2 \varphi \right] + H(A). \quad (7)$$

2.3. CGLE in the spherical coordinates

Let us consider a three dimensional (3D) spherical coordinate system (r, φ, θ) , see Fig. 1(b). The spherical coordinates translate into the Cartesian coordinates by $x = r \sin \varphi \cos \theta, y = r \sin \varphi \sin \theta, z = r \cos \varphi, (0 < \varphi < \pi, 0 \leq \theta \leq 2\pi)$. In the spherical coordinates, the CGLE transforms into the following form

$$\frac{\partial A}{\partial t} = \beta \left[\frac{\partial^2 A}{\partial r^2} + \frac{\partial^2}{\partial \varphi^2} \left(\frac{A}{r^2} \right) + \frac{\partial^2}{\partial \theta^2} \left(\frac{A}{r^2 \sin^2 \varphi} \right) \right] + S(A), \quad (8)$$

where the source term is

$$S(A) = 2\beta \frac{\partial}{\partial r} \left(\frac{A}{r} \right) + \beta \frac{\partial}{\partial \varphi} \left(\frac{\operatorname{ctg}\varphi A}{r^2} \right) + \frac{\beta \csc^2 \varphi A}{r^2} + 2\beta \frac{A}{r^2} + H(A). \quad (9)$$

2.4. Complex lattice Boltzmann model

In the 2D space which consists of r -axis and θ -axis, we adopt the standard D2Q9 lattice, see Fig. 1(a). The cell position indicated by \mathbf{x} is expressed as (r, θ) . Its nearest neighboring cell is located at $\mathbf{x} + \mathbf{e}_\alpha, \alpha = 0, 1, \dots, b$. The lattice Boltzmann model can be regarded as that whose lattice has b links that connect the center site to its b neighboring nodes. The complex distribution function $F_\alpha(\mathbf{x}, t)$ is defined at position \mathbf{x} , time t , with velocity \mathbf{e}_α . The particles velocity \mathbf{e}_α is divided into eight directions, it is expressed as

$$\mathbf{e}_\alpha = c \begin{pmatrix} 0 & 1 & -1 & 0 & 0 & 1 & -1 & 1 & -1 \\ 0 & 0 & 0 & 1 & -1 & 1 & -1 & -1 & 1 \end{pmatrix}. \quad (10)$$

Spherical surface is still a 2D space which consists of φ -axis and θ -axis. We also adopt the standard D2Q9 lattice as shown in Fig. 1(a). In the numerical simulation, we set $R = 1$.

In the 3D space, we adopt the standard D3Q15 lattice with a cell position indicated by \mathbf{x} expressed as (r, φ, θ) , as shown in Fig. 1(c). In this 3D lattice, the particles velocity \mathbf{e}_α is divided into fourteen directions, it is expressed as

$$\mathbf{e}_\alpha = c \begin{pmatrix} 0 & 1 & -1 & 0 & 0 & 0 & 0 & 1 & -1 & 1 & -1 & 1 & -1 & -1 & 1 \\ 0 & 0 & 0 & 1 & -1 & 0 & 0 & 1 & -1 & 1 & -1 & 1 & -1 & 1 & 1 & -1 \\ 0 & 0 & 0 & 0 & 0 & 1 & -1 & 1 & -1 & -1 & 1 & 1 & -1 & 1 & 1 & -1 \end{pmatrix}. \quad (11)$$

The complex quantity $A(\mathbf{x}, t)$ is defined as follows

$$A(\mathbf{x}, t) = \sum_{\alpha} F_{\alpha}(\mathbf{x}, t). \quad (12)$$

In order to obtain an available macroscopic quantity $A(\mathbf{x}, t)$, we assume that the distribution $F_{\alpha}(\mathbf{x}, t)$ has local equilibrium distribution function $F_{\alpha}^{eq}(\mathbf{x}, t)$, which satisfies

$$\sum_{\alpha} F_{\alpha}^{eq}(\mathbf{x}, t) = A(\mathbf{x}, t). \quad (13)$$

The lattice Boltzmann equation is

$$F_{\alpha}(\mathbf{x} + \mathbf{e}_{\alpha}, t + 1) - F_{\alpha}(\mathbf{x}, t) = -\frac{1}{\tau} [F_{\alpha}(\mathbf{x}, t) - F_{\alpha}^{eq}(\mathbf{x}, t)] + \Omega_{\alpha}^R(\mathbf{x}, t), \quad (14)$$

where τ is the single relaxation time factor which is a real constant. The complex variable $\Omega_{\alpha}^R(\mathbf{x}, t)$ is assumed as

$$\Omega_{\alpha}^R = \sum_{i=1}^3 \varepsilon^i \Omega_{\alpha}^{(i)} + O(\varepsilon^4), \quad (15)$$

where ε is Knudsen number. The Knudsen number ε is defined as $\varepsilon = \frac{l}{L}$, here l is the mean free path, and L is the characteristic length. It is convenient that ε equals to the time step Δt in numerical simulations. Thus, the lattice Boltzmann equation in physical unit is

$$F_{\alpha}(\mathbf{x} + \varepsilon \mathbf{e}_{\alpha}, t + \varepsilon) - F_{\alpha}(\mathbf{x}, t) = -\frac{1}{\tau} [F_{\alpha}(\mathbf{x}, t) - F_{\alpha}^{eq}(\mathbf{x}, t)] + \Omega_{\alpha}^R(\mathbf{x}, t). \quad (16)$$

The Chapman–Enskog expansion is applied to the real part and the imagery part of $F_\alpha(\mathbf{x}, t)$ under the assumption of small Knudsen number ε , and we have

$$F_\alpha = \sum_{n=0}^{\infty} \varepsilon^n F_\alpha^{(n)}. \quad (17)$$

In Eq. (17), $F_\alpha^{(0)}$ denotes $F_\alpha^{eq}(\mathbf{x}, t)$. We discuss the changes in different time scales, introduced as t_0, t_1, \dots , they are

$$t_n = \varepsilon^n t, \quad n = 0, 1, \dots, \quad (18)$$

and

$$\frac{\partial}{\partial t} = \sum_{m=0}^3 \varepsilon^m \frac{\partial}{\partial t_m} + O(\varepsilon^4). \quad (19)$$

By using the Taylor expansion on Eq. (16), and retaining terms up to $O(\varepsilon^4)$, and combine with Eqs. (17), and (19), we obtain a series of partial differential equations as follows

$$\Delta F_\alpha^{(0)} = -\frac{1}{\tau} F_\alpha^{(1)} + \Omega_\alpha^{(1)}, \quad (20)$$

$$\frac{\partial}{\partial t_1} F_\alpha^{(0)} + C_2 \Delta^2 F_\alpha^{(0)} + \tau \Delta \Omega_\alpha^{(1)} = -\frac{1}{\tau} F_\alpha^{(2)} + \Omega_\alpha^{(2)}, \quad (21)$$

$$C_3 \Delta^3 F_\alpha^{(0)} + 2C_2 \frac{\partial}{\partial t_1} \Delta F_\alpha^{(0)} + \frac{\partial}{\partial t_2} F_\alpha^{(0)} + \tau C_2 \Delta^2 \Omega_\alpha^{(1)} + \tau \frac{\partial}{\partial t_1} \Omega_\alpha^{(1)} + \tau \Delta \Omega_\alpha^{(2)} = -\frac{1}{\tau} F_\alpha^{(3)} + \Omega_\alpha^{(3)}, \quad (22)$$

$$\begin{aligned} & C_4 \Delta^4 F_\alpha^{(0)} + 3C_3 \frac{\partial}{\partial t_1} \Delta^2 F_\alpha^{(0)} + 2C_2 \frac{\partial}{\partial t_2} \Delta F_\alpha^{(0)} + \frac{\partial}{\partial t_3} F_\alpha^{(0)} + C_2 \frac{\partial^2}{\partial t_1^2} F_\alpha^{(0)} \\ & + \tau C_3 \Delta^3 \Omega_\alpha^{(1)} + 2\tau C_2 \frac{\partial}{\partial t_1} \Delta \Omega_\alpha^{(1)} + \tau \frac{\partial}{\partial t_2} \Omega_\alpha^{(1)} + \tau C_2 \Delta^2 \Omega_\alpha^{(2)} + \tau \frac{\partial}{\partial t_1} \Omega_\alpha^{(2)} + \tau \Delta \Omega_\alpha^{(3)} = -\frac{1}{\tau} F_\alpha^{(4)} + \Omega_\alpha^{(4)}, \end{aligned} \quad (23)$$

where operator $\Delta = \frac{\partial}{\partial t_0} + \mathbf{e}_\alpha \frac{\partial}{\partial \mathbf{x}}$, the coefficients C_i are

$$C_i = \sum_{k=1}^{i-1} \frac{(-\tau C_k)}{(i-k)!} + \frac{1}{i!}, \quad i = 1, 2, 3, 4. \quad (24)$$

For the 2D models, we select that

$$\sum_{\alpha=0}^b F_\alpha^{eq} = A, \quad (25a)$$

$$\sum_{\alpha=1}^b F_\alpha^{eq} e_{\alpha i} = 0, \quad (25b)$$

$$\sum_{\alpha=1}^b F_\alpha^{eq} e_{\alpha j} = 0, \quad (25c)$$

$$\sum_{\alpha=1}^b F_\alpha^{eq} e_{\alpha i} e_{\alpha i} = \beta^0 c^2 A, \quad (25d)$$

$$\sum_{\alpha=1}^b F_\alpha^{eq} e_{\alpha j} e_{\alpha j} = \gamma^0 c^2 A, \quad (25e)$$

$$\sum_{\alpha=1}^b F_\alpha^{eq} e_{\alpha i} e_{\alpha j} = 0, \quad (25f)$$

where $\beta^0 = \frac{\beta}{-C_2 \varepsilon c^2}$, $\gamma^0 = \frac{\beta}{-C_2 \varepsilon c^2 r^2}$, $i = r, j = \theta$ for the polar coordinate and $\beta^0 = \frac{\beta}{-C_2 \varepsilon c^2}$, $\gamma^0 = \frac{\beta}{-C_2 \varepsilon c^2} \csc^2 \varphi$, $i = \varphi, j = \theta$ for the spherical surface coordinates. The equilibrium distribution function can be obtained as

$$F_0^{eq} = A(1 - \gamma^0), \quad (26a)$$

$$F_1^{eq} = 0, \quad (26b)$$

$$F_2^{eq} = 0, \quad (26c)$$

$$F_3^{eq} = F_4^{eq} = \frac{\gamma^0 - \beta^0}{2} A, \quad (26d)$$

$$F_5^{eq} = F_6^{eq} = F_7^{eq} = F_8^{eq} = \frac{\beta^0}{4} A. \quad (26e)$$

For the 3D model, we select that

$$\sum_{\alpha=0}^b F_{\alpha}^{eq} = A, \quad (27a)$$

$$\sum_{\alpha=1}^b F_{\alpha}^{eq} e_{\alpha r} = 0, \quad (27b)$$

$$\sum_{\alpha=1}^b F_{\alpha}^{eq} e_{\alpha\varphi} = 0, \quad (27c)$$

$$\sum_{\alpha=1}^b F_{\alpha}^{eq} e_{\alpha\theta} = 0, \quad (27d)$$

$$\sum_{\alpha=1}^b F_{\alpha}^{eq} e_{\alpha r} e_{\alpha r} = \beta^0 c^2 A, \quad (27e)$$

$$\sum_{\alpha=1}^b F_{\alpha}^{eq} e_{\alpha\phi} e_{\alpha\phi} = \gamma^0 c^2 A, \quad (27f)$$

$$\sum_{\alpha=1}^b F_{\alpha}^{eq} e_{\alpha\theta} e_{\alpha\theta} = \lambda^0 c^2 A, \quad (27g)$$

$$\sum_{\alpha=1}^b F_{\alpha}^{eq} e_{\alpha r} e_{\alpha\varphi} = 0, \quad (27h)$$

$$\sum_{\alpha=1}^b F_{\alpha}^{eq} e_{\alpha\phi} e_{\alpha\theta} = 0, \quad (27i)$$

$$\sum_{\alpha=1}^b F_{\alpha}^{eq} e_{\alpha\theta} e_{\alpha r} = 0, \quad (27j)$$

where $\beta^0 = \frac{\beta}{-C_2 \varepsilon c^2}$, $\gamma^0 = \frac{\beta}{-C_2 \varepsilon c^2 r^2}$, $\lambda^0 = \frac{\beta}{-C_2 \varepsilon c^2 r^2} \csc^2 \varphi$. The equilibrium distribution function can be obtained as

$$F_0^{eq} = A(1 - \lambda^0 - \gamma^0), \quad (28a)$$

$$F_1^{eq} = F_2^{eq} = \frac{\beta^0}{4} A, \quad (28b)$$

$$F_3^{eq} = F_4^{eq} = \frac{1}{2} \left[\gamma^0 - \frac{\beta^0}{2} \right] A, \quad (28c)$$

$$F_5^{eq} = F_6^{eq} = \frac{1}{2} \left(\lambda^0 - \frac{\beta^0}{2} \right) A, \quad (28d)$$

$$F_7^{eq} = \dots = F_{14}^{eq} = \frac{\beta^0}{16} A. \quad (28e)$$

By using the partial differential equation (20), we have the conservation law in scale t_0

$$\frac{\partial A}{\partial t_0} = 0. \quad (29)$$

We assume that

$$\Omega_{\alpha}^{(n)} = 0, n \neq 2. \quad (30)$$

And note

$$\sum_{\alpha} \Omega_{\alpha}^{(2)} \equiv \phi. \quad (31)$$

According to Eq. (21) and the moment's equations (25), (27), we have the partial differential equations in scale t_1 as follows:
For polar coordinates

$$\frac{\partial A}{\partial t_1} + C_2 \left(\frac{\partial^2 \beta^0 c^2 A}{\partial r^2} + \frac{\partial^2 \gamma^0 c^2 A}{\partial \theta^2} \right) = \phi. \quad (32)$$

For spherical surface coordinates

$$\frac{\partial A}{\partial t_1} + C_2 \left(\frac{\partial^2 \beta^0 c^2 A}{\partial \varphi^2} + \frac{\partial^2 \gamma^0 c^2 A}{\partial \theta^2} \right) = \phi. \quad (33)$$

For 3D spherical coordinates

$$\frac{\partial A}{\partial t_1} + C_2 \left(\frac{\partial^2 \beta^0 c^2 A}{\partial r^2} + \frac{\partial^2 \gamma^0 c^2 A}{\partial \varphi^2} + \frac{\partial^2 \lambda^0 c^2 A}{\partial \theta^2} \right) = \phi. \quad (34)$$

Taking (20) + (21) $\times \varepsilon$ + (22) $\times \varepsilon^2$ + (23) $\times \varepsilon^3$ and set $\varepsilon\phi = S(A)$, the CGLE is recovered in polar coordinates as following form

$$\frac{\partial A}{\partial t} = \beta \left[\frac{\partial^2 A}{\partial r^2} + \frac{\partial^2}{\partial \theta^2} \left(\frac{A}{r^2} \right) \right] + S(A) + E_2 + E_3 + O(\varepsilon^4). \quad (35)$$

The CGLE in spherical surface coordinates is

$$\frac{\partial A}{\partial t} = \frac{\beta}{R^2} \left[\frac{\partial^2 A}{\partial \varphi^2} + \frac{\partial^2}{\partial \theta^2} \left(\frac{A}{\sin^2 \varphi} \right) \right] + S(A) + E_2 + E_3 + O(\varepsilon^4). \quad (36)$$

The CGLE in 3D spherical coordinates is

$$\frac{\partial A}{\partial t} = \beta \left[\frac{\partial^2 A}{\partial r^2} + \frac{\partial^2}{\partial \varphi^2} \left(\frac{A}{r^2} \right) + \frac{\partial^2}{\partial \theta^2} \left(\frac{A}{r^2 \sin^2 \varphi} \right) \right] + S(A) + E_2 + E_3 + O(\varepsilon^4). \quad (37)$$

The source terms $S(A)$ in (35)–(37) are expressed as Eqs. (3), (7), (9), respectively. The error term E_2 is

$$E_2 = -\varepsilon^2 \sum_{\alpha} \left[C_3 \Delta^3 F_{\alpha}^{(0)} + 2C_2 \frac{\partial}{\partial t_1} \Delta F_{\alpha}^{(0)} + \tau \Delta \Omega_{\alpha}^{(2)} \right]. \quad (38)$$

According to (29), we have

$$\frac{\partial S(A)}{\partial t_0} = 0. \quad (39)$$

The third order moment $\sum_{\alpha} F_{\alpha}^{eq} e_{\alpha i} e_{\alpha j} e_{\alpha k}$ can be obtained by the equilibrium distribution functions as

$$\sum_{\alpha} F_{\alpha}^{eq} e_{\alpha i} e_{\alpha j} e_{\alpha k} = 0. \quad (40)$$

If we set

$$\psi_i^{(2)} \equiv \sum_{\alpha} \Omega_{\alpha}^{(2)} e_{\alpha i} = 0. \quad (41)$$

The error term E_2 is

$$E_2 = 0. \quad (42)$$

The error term E_3 is

$$E_3 = -\varepsilon^3 \sum_{\alpha} \left[C_4 \Delta^4 F_{\alpha}^{(0)} + 3C_3 \frac{\partial}{\partial t_1} \Delta^2 F_{\alpha}^{(0)} + C_2 \frac{\partial^2}{\partial t_1^2} F_{\alpha}^{(0)} + \tau C_2 \Delta^2 \Omega_{\alpha}^{(2)} + \tau \frac{\partial}{\partial t_1} \Omega_{\alpha}^{(2)} \right]. \quad (43)$$

The fourth order moment $\sum_{\alpha} F_{\alpha}^{eq} e_{\alpha i} e_{\alpha j} e_{\alpha k} e_{\alpha m}$ for the polar coordinates can be obtained as

$$\sum_{\alpha=1}^b F_{\alpha}^{eq} e_{\alpha r} e_{\alpha r} e_{\alpha r} e_{\alpha r} = \beta^0 c^4 A, \quad (44a)$$

$$\sum_{\alpha=0}^b F_{\alpha}^{eq} e_{\alpha r} e_{\alpha r} e_{\alpha r} e_{\alpha \theta} = 0, \quad (44b)$$

$$\sum_{\alpha=0}^b F_{\alpha}^{eq} e_{\alpha r} e_{\alpha r} e_{\alpha \theta} e_{\alpha \theta} = \beta^0 c^4 A, \quad (44c)$$

$$\sum_{\alpha=0}^b F_{\alpha}^{eq} e_{\alpha r} e_{\alpha \theta} e_{\alpha \theta} e_{\alpha \theta} = 0, \quad (44d)$$

$$\sum_{\alpha=0}^b F_{\alpha}^{eq} e_{\alpha \theta} e_{\alpha \theta} e_{\alpha \theta} e_{\alpha \theta} = \gamma^0 c^4 A. \quad (44e)$$

Set

$$\psi_{rr}^{(2)} \equiv \sum_{\alpha} \Omega_{\alpha}^{(2)} e_{\alpha r} e_{\alpha r} = -\frac{1}{\tau C_2} (3C_3 - C_2 C_2) \beta^0 c^2 \phi, \quad (45a)$$

$$\psi_{r\theta}^{(2)} \equiv \sum_{\alpha} \Omega_{\alpha}^{(2)} e_{\alpha r} e_{\alpha \theta} = 0, \quad (45b)$$

$$\psi_{\theta\theta}^{(2)} \equiv \sum_{\alpha} \Omega_{\alpha}^{(2)} e_{\alpha \theta} e_{\alpha \theta} = -\frac{1}{\tau C_2} (3C_3 - C_2 C_2) \gamma^0 c^2 \phi. \quad (45c)$$

The additional distribution is

$$\Omega_0^{(2)} = \phi \left[1 + \frac{1}{\tau C_2} (3C_3 - C_2 C_2) \gamma^0 \right], \quad (46a)$$

$$\Omega_1^{(2)} = \Omega_2^{(2)} = 0, \quad (46b)$$

$$\Omega_3^{(2)} = \Omega_4^{(2)} = 0.5 \left[-\frac{1}{\tau C_2} (3C_3 - C_2 C_2) (\gamma^0 - \beta^0) \right] \phi, \quad (46c)$$

$$\Omega_5^{(2)} = \Omega_6^{(2)} = \Omega_7^{(2)} = \Omega_8^{(2)} = 0.25 \left[-\frac{1}{\tau C_2} (3C_3 - C_2 C_2) \beta^0 \right] \phi, \quad (46d)$$

where $\beta^0 = \frac{\beta}{-C_2 \varepsilon c^2}$, $\gamma^0 = \frac{\beta}{-C_2 \varepsilon c^2 r^2}$. The E_3 in the polar coordinates is

$$E_3 = -\varepsilon^3 \left\{ c^4 \beta^0 [C_4 - C_2 (3C_3 - C_2 C_2) \beta^0] \frac{\partial^4 A}{\partial r^4} + c^4 \beta^0 [6C_4 - 2C_2 (3C_3 - C_2 C_2) \gamma^0] \frac{\partial^4 A}{\partial \theta^2 \partial r^2} \right. \\ \left. + c^4 \gamma^0 [C_4 - C_2 (3C_3 - C_2 C_2) \gamma^0] \frac{\partial^4 A}{\partial \theta^4} + c^4 \gamma^0 \gamma^0 C_2 (3C_3 - C_2 C_2) \frac{\partial^2}{\partial \theta^2} \left(4r \frac{\partial A}{\partial r} - 6A \right) + 0.5 \frac{\partial}{\partial t_1} \phi \right\}. \quad (47)$$

Similarly, in the spherical surface coordinates, the additional distribution has the same form as (46) with $\beta^0 = \frac{\beta}{-C_2 \varepsilon c^2 R^2}$, $\gamma^0 = \frac{\beta}{-C_2 \varepsilon c^2 R^2} \csc^2 \varphi$. The error term E_3 is

$$E_3 = -\varepsilon^3 \left\{ \beta^0 c^4 [C_4 - (3C_3 - C_2 C_2) C_2 \beta^0] \frac{\partial^2}{\partial \varphi^2} \frac{\partial^2 A}{\partial \varphi^2} + \beta^0 c^4 [6C_4 - 2(3C_3 - C_2 C_2) C_2 \gamma^0] \frac{\partial^2}{\partial \varphi^2} \frac{\partial^2 A}{\partial \theta^2} \right. \\ \left. + \gamma^0 c^4 [C_4 - (3C_3 - C_2 C_2) C_2 \gamma^0] \frac{\partial^2}{\partial \theta^2} \frac{\partial^2 A}{\partial \theta^2} \right. \\ \left. + (3C_3 - C_2 C_2) C_2 c^4 \gamma^0 \frac{\partial^2}{\partial \theta^2} \left[4 \cos \varphi \sin \varphi \frac{\partial A}{\partial \varphi} - (6 - 8 \sin^2 \varphi) A \right] + 0.5 \frac{\partial}{\partial t_1} \phi \right\}. \quad (48)$$

The fourth order moment $\sum_{\alpha} F_{\alpha}^{eq} e_{\alpha i} e_{\alpha j} e_{\alpha k} e_{\alpha m}$ for the 3D spherical coordinates can be obtained as

$$\sum_{\alpha=1}^b F_{\alpha}^{eq} e_{\alpha r} e_{\alpha r} e_{\alpha r} e_{\alpha r} = \beta^0 c^4 A, \quad (49a)$$

$$\sum_{\alpha=0}^b F_{\alpha}^{eq} e_{\alpha\varphi} e_{\alpha\varphi} e_{\alpha\varphi} e_{\alpha\varphi} = \gamma^0 c^4 A, \quad (49b)$$

$$\sum_{\alpha=0}^b F_{\alpha}^{eq} e_{\alpha\theta} e_{\alpha\theta} e_{\alpha\theta} e_{\alpha\theta} = \lambda^0 c^4 A, \quad (49c)$$

$$\sum_{\alpha=0}^b F_{\alpha}^{eq} e_{\alpha r} e_{\alpha r} e_{\alpha\varphi} e_{\alpha\varphi} = \sum_{\alpha=0}^b F_{\alpha}^{eq} e_{\alpha\varphi} e_{\alpha\varphi} e_{\alpha\theta} e_{\alpha\theta} = \sum_{\alpha=0}^b F_{\alpha}^{eq} e_{\alpha r} e_{\alpha r} e_{\alpha\theta} e_{\alpha\theta} = \frac{\beta^0 c^4 A}{2}. \quad (49d)$$

The other components of this moment are zero. Set

$$\psi_{rr}^{(2)} \equiv \sum_{\alpha} \Omega_{\alpha}^{(2)} e_{\alpha r} e_{\alpha r} = -\frac{1}{\tau C_2} (3C_3 - C_2 C_2) \beta^0 c^2 \phi, \quad (50a)$$

$$\psi_{r\theta}^{(2)} \equiv \sum_{\alpha} \Omega_{\alpha}^{(2)} e_{\alpha r} e_{\alpha\theta} = 0, \quad (50b)$$

$$\psi_{\varphi\varphi}^{(2)} \equiv \sum_{\alpha} \Omega_{\alpha}^{(2)} e_{\alpha\varphi} e_{\alpha\varphi} = -\frac{1}{\tau C_2} (3C_3 - C_2 C_2) \gamma^0 c^2 \phi, \quad (50c)$$

$$\psi_{\varphi\theta}^{(2)} \equiv \sum_{\alpha} \Omega_{\alpha}^{(2)} e_{\alpha\varphi} e_{\alpha\theta} = 0, \quad (50d)$$

$$\psi_{\theta\theta}^{(2)} \equiv \sum_{\alpha} \Omega_{\alpha}^{(2)} e_{\alpha\theta} e_{\alpha\theta} = -\frac{1}{\tau C_2} (3C_3 - C_2 C_2) \lambda^0 c^2 \phi, \quad (50e)$$

$$\psi_{r\varphi}^{(2)} \equiv \sum_{\alpha} \Omega_{\alpha}^{(2)} e_{\alpha r} e_{\alpha\varphi} = 0. \quad (50f)$$

The additional distribution is

$$\Omega_0^{(2)} = \phi \left[1 + \frac{1}{\tau C_2} (3C_3 - C_2 C_2) (\gamma^0 + \lambda^0) \right], \quad (51a)$$

$$\Omega_1^{(2)} = \Omega_2^{(2)} = \frac{1}{4} \left[-\frac{1}{\tau C_2} (3C_3 - C_2 C_2) \beta^0 \right] \phi, \quad (51b)$$

$$\Omega_3^{(2)} = \Omega_4^{(2)} = \frac{1}{2} \left[-\frac{1}{\tau C_2} (3C_3 - C_2 C_2) \left(\gamma^0 - \frac{\beta^0}{2} \right) \right] \phi, \quad (51c)$$

$$\Omega_5^{(2)} = \Omega_6^{(2)} = \frac{1}{2} \left[-\frac{1}{\tau C_2} (3C_3 - C_2 C_2) \left(\lambda^0 - \frac{\beta^0}{2} \right) \right] \phi, \quad (51d)$$

$$\Omega_7^{(2)} = \dots = \Omega_{14}^{(2)} = \frac{1}{16} \left[-\frac{1}{\tau C_2} (3C_3 - C_2 C_2) \beta^0 \right] \phi, \quad (51e)$$

where $\beta^0 = \frac{\beta}{-C_2 \varepsilon c^2}$, $\gamma^0 = \frac{\beta}{-C_2 \varepsilon c^2 r^2}$, $\lambda^0 = \frac{\beta}{-C_2 \varepsilon c^2 r^2} \csc^2 \varphi$. The E_3 in 3D spherical coordinates is

$$\begin{aligned} E_3 = & -\varepsilon^3 c^4 \left\{ [C_4 \beta^0 - (3C_3 - C_2 C_2) C_2 \beta^0 \beta^0] \frac{\partial^4 A}{\partial r^4} + [C_4 \gamma^0 - (3C_3 - C_2 C_2) C_2 \gamma^0 \gamma^0] \frac{\partial^4 A}{\partial \varphi^4} \right. \\ & + [C_4 \lambda^0 - (3C_3 - C_2 C_2) C_2 \lambda^0 \lambda^0] \frac{\partial^4 A}{\partial \theta^4} + [3C_4 \beta^0 - 2(3C_3 - C_2 C_2) C_2 \lambda^0 \beta^0] \frac{\partial^4 A}{\partial r^2 \partial \theta^2} \\ & + [3C_4 \beta^0 - 2(3C_3 - C_2 C_2) C_2 \beta^0 \gamma^0] \frac{\partial^4 A}{\partial r^2 \partial \varphi^2} + [3C_4 \beta^0 - 2(3C_3 - C_2 C_2) C_2 \lambda^0 \gamma^0] \frac{\partial^4 A}{\partial \varphi^2 \partial \theta^2} \\ & + c^4 \lambda^0 \gamma^0 C_2 (3C_3 - C_2 C_2) \frac{\partial^2}{\partial \theta^2} \left(4r \frac{\partial A}{\partial r} - 6A \right) + c^4 \gamma^0 \gamma^0 C_2 (3C_3 - C_2 C_2) \frac{\partial^2}{\partial \varphi^2} \left(4r \frac{\partial A}{\partial r} - 6A \right) \\ & \left. + (3C_3 - C_2 C_2) C_2 c^4 \lambda^0 \lambda^0 \frac{\partial^2}{\partial \theta^2} \left[4 \cos \varphi \sin \varphi \frac{\partial A}{\partial \varphi} - (6 - 8 \sin^2 \varphi) A \right] + 0.5 \frac{\partial}{\partial t_1} \phi \right\}. \end{aligned} \quad (52)$$

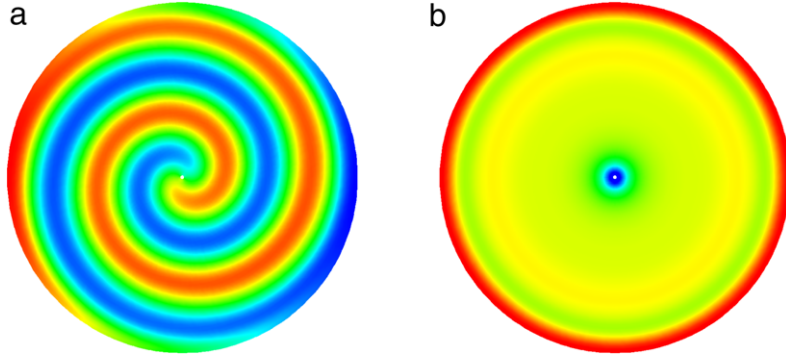


Fig. 2. (Color online) Patterns for a single stable spiral wave in CGLE by using the LBM, (a) $\text{Re}(A)$ and (b) $|A|$ at time $t = 50$. The parameters are: $\beta = 0.001(1 - 1.35i)$, $a = 1$, $d = 1 + 0.34i$, lattice size 50×300 , $\Delta r = \Delta\theta = \frac{2\pi}{300}$, $\tau = 1.0$, $c = 100\pi$.

3. Numerical examples

3.1. Spiral wave in the circular domain

To test the correctness and applicability of the approach described above, we perform simulations on CGLE with spiral waves. We select the computing region as $0 < r \leq 1$, $0 \leq \theta < 2\pi$ with lattice size $M \times N$. The space step is set as $\Delta r = \Delta\theta = 2\pi/N$, thus M is nearly $\frac{N}{6}$. In the simulation, $N = 300$. The boundary conditions are the periodic boundary condition for θ , and Neumann boundary condition for r , respectively. The initial condition is set as

$$A(r, \theta, 0) = pr(\cos \theta + i \sin \theta). \quad (53)$$

In Eq. (53), p is selected as $\frac{1}{\pi}$.

This initial condition will create a phase singularity at the center of the region and will form a spiral wave, as is shown in Fig. 2. Fig. 2(a) is the real part of $A(r, \theta)$ at time $t = 50$ by using the LBM in polar coordinates. It shows a spiral that can be fitted by Archimedean spiral far from the core. Fig. 2(b) gives the pattern of $|A|$ at the same time which shows the singularity.

In order to compute the truncation error of the LBM, we employ the numerical result of a kind of finite difference scheme. The finite difference scheme in the polar coordinates is

$$\begin{aligned} \frac{A_{i,j}^{k+1} - A_{i,j}^k}{\Delta t} &= \frac{\beta}{\Delta r^2 r_i} [r_{i+0.5}(A_{i+1,j}^k - A_{i,j}^k) - r_{i-0.5}(A_{i,j}^k - A_{i,j-1}^k)] \\ &\quad + \frac{\beta}{\Delta\theta^2 r_i^2} [A_{i,j+1}^k - 2A_{i,j}^k + A_{i,j-1}^k] + H(A_{i,j}^k), \end{aligned} \quad (54)$$

where $\Delta r = \Delta\theta = 2\pi/N$, $A_{i,j}^k = A((i - 0.5)\Delta r, j\Delta\theta, k\Delta t)$, $r_i = (i - 0.5)\Delta r$, $i = 1, \dots, M$, $j = 0, 1, \dots, N - 1$. This difference scheme has the accuracy of $O(\Delta t + \Delta r^2)$. We define the relative error as

$$E_r = \frac{|A^L - A^E|}{|A^E|}, \quad (55)$$

where A^L is the LBM result, and A^E is the result by finite difference scheme. In the simulations, the space step and time step of the finite difference scheme are set the same as that of LBM. In Fig. 3(a), we give the comparison of the results by the two methods on $\theta = \pi$ at $t = 50$. The parameters are the same as Fig. 2. The results agree well with each other. Fig. 3(b) shows the relative error versus coordinate r at the same time and position. From Fig. 3(b), we find that LBM results are close to the finite difference scheme results.

The general relative error is defined as

$$G = \frac{\sum_{j=1}^N \sum_{i=1}^M |A^L - A^E|}{\sum_{j=1}^N \sum_{i=1}^M |A^E|} \quad (56)$$

where A^N is the LBM result, and A^E is the result by finite difference scheme. Fig. 3(c) shows the relation between the general relative error and the lattice size. It provides a qualitative trend of the convergence of the LBM. By employing the regression fit, the line is $\log_{10} G = 1.841 \log_{10} \Delta x - 0.205$, say, the slope of this relative error curve is 1.841, and the order of the

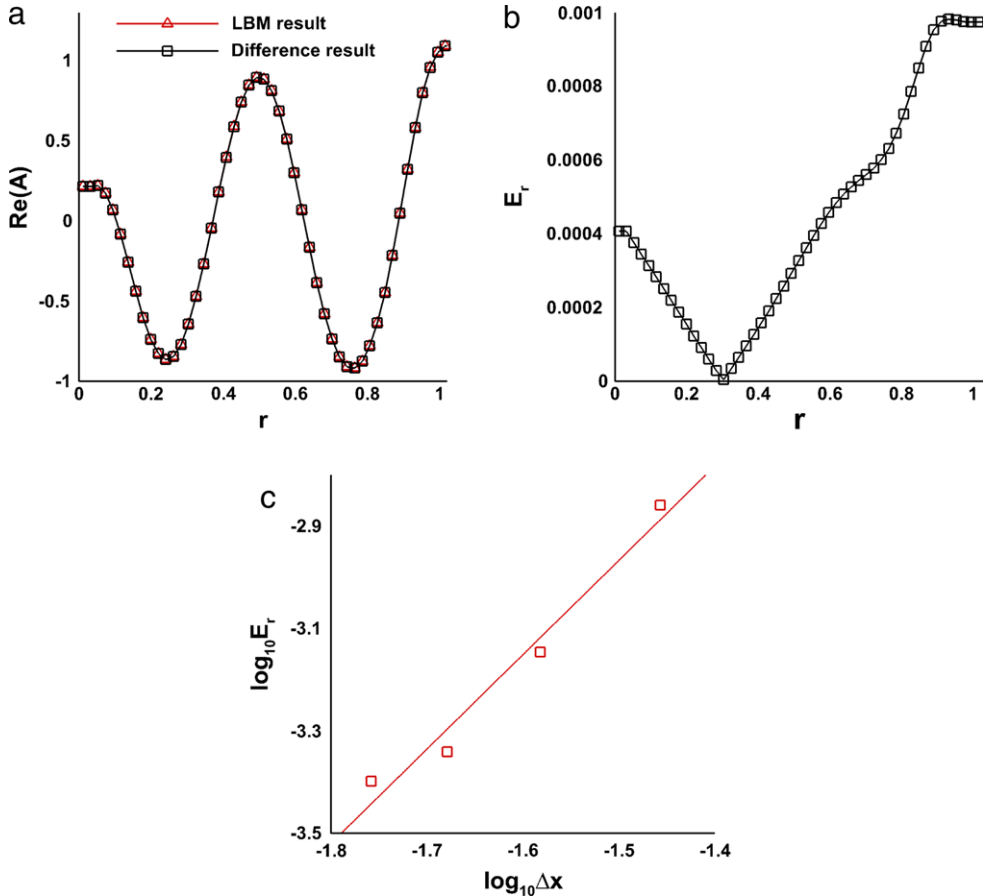


Fig. 3. (Color online) (a) The comparison of the LBM result and finite difference scheme result versus coordinate r on $\theta = \pi$ at $t = 50$. (b) The relative error at the same time and position. Parameters are the same as that in Fig. 2. (c) The Log–Log curve of the general relative errors versus space step Δx at $t = 50$. The parameters are the same as Fig. 2 except for Δx .

Table 1
Comparison of CPU time cost by LBM and finite difference scheme, the unit is second. The parameters are the same as Fig. 3(c).

Lattice number	30×180	40×240	50×300	60×360
LBM	145	428	1414	5650
Difference scheme	40	126	592	1656

numerical convergence of the algorithm is also 1.841 for Δx . The qualitative trend of the convergence of the LBM algorithm is acceptable. The results show that the LBM model is basically equivalent to the finite difference scheme.

In Table 1, the comparison of CPU time cost by the LBM and finite difference scheme at $t = 50$ is listed. The CPU time cost by LBM is more than that by the finite difference scheme. But the stability of LBM is better than the finite difference scheme under the condition of the singularity at $r = 0$. The boundary at $r = 1$ by LBM can also be treated as bounce back boundary conditions which will give better results than the finite difference scheme. As to the stability, the relaxation factor τ need to greater than 0.5, and in the simulations we will find that its region is about (0.85, 1.5).

Another initial condition is set as

$$A(r, \theta, 0) = p(u + iv). \quad (57)$$

In Eq. (57), p is selected as $\frac{1}{\pi}$, and u, v are values selected in $[-0.5, 0.5]$ randomly.

This is an unstable initial condition which will create many phase singularities. Under such condition, multi-spiral waves can be created as shown in Fig. 4. And as time goes on, the number of singularities deceases, at last, a frozen state is formed. Fig. 4 shows the multi-spiral waves of $\text{Re}(A)$ with different diffusion coefficient β from $t = 100$ to $t = 1800$. It is seen that the numerical results agree well with those in Ref. [7].

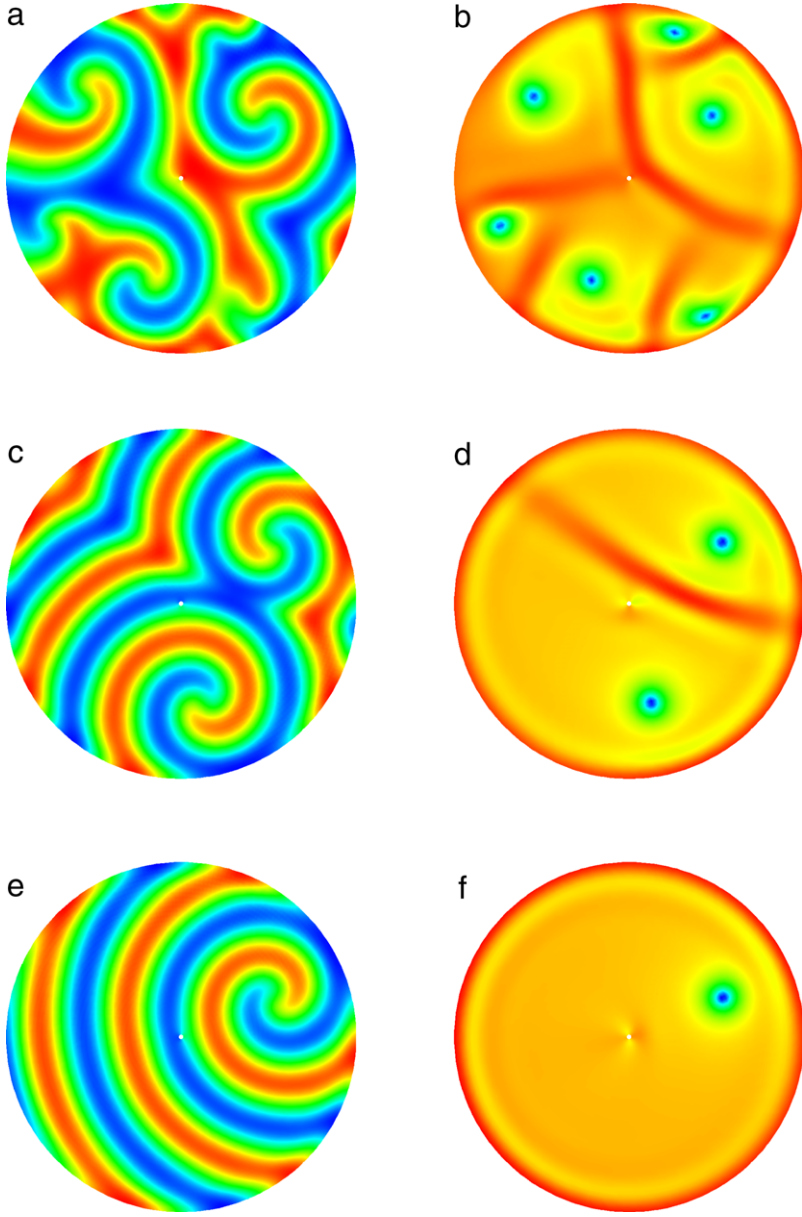


Fig. 4. (Color online) Patterns of $\text{Re}(A)$ and $|A|$ for stable spiral wave with unstable initial condition at $t = 100$, $t = 600$, and $t = 1800$. (a) $\text{Re}(A)$ at $t = 100$ (b) $|A|$ at $t = 100$ (c) $\text{Re}(A)$ at $t = 600$ (d) $|A|$ at $t = 600$ (e) $\text{Re}(A)$ at $t = 1800$ (f) $|A|$ at $t = 1800$. Parameters are the same as Fig. 2.

The third initial condition is set as

$$A(r, \theta, 0) = \begin{cases} r \sin \theta + (r \cos \theta - 0.5)i, & \theta \in \left[0, \frac{\pi}{2}\right] \cup \left[\frac{3\pi}{2}, 2\pi\right), \\ r \sin(\pi - \theta) + [r \cos(\pi - \theta) - 0.5]i, & \theta \in \left(\frac{\pi}{2}, \frac{3\pi}{2}\right). \end{cases} \quad (58)$$

This initial condition can create two opposite phase singularities. Thus, as times goes on, a pair of spiral waves will appear, as shown in Fig. 5. Fig. 5(a) gives the $\text{Re}(A)$ pattern of spiral waves in a circular domain, (b) shows the $|A|$ pattern of two singularities. Fig. 5(c) is the pattern of $\text{Re}(A)$ at $\theta = 0$ and $\theta = \pi$ denoted by x from $t = 50$ to $t = 100$. This pattern shows the two spiral waves are inwardly rotating.

Next, we will test the influence of parameters. Here, we will give six sets of tests. Firstly, we test the imaginary part of d with keeping the diffusion coefficient $\beta = 0.001(1 - 1.35i)$ and the linear term coefficient $a = 1$. Fig. 6 gives the patterns of $\text{Re}(A)$ at $\theta = 0$ from $t = 60$ to $t = 110$ with the $\text{Im}(d)$ changing as $-0.2, 0, 0.2, 0.5$, and 1 , respectively. These patterns are

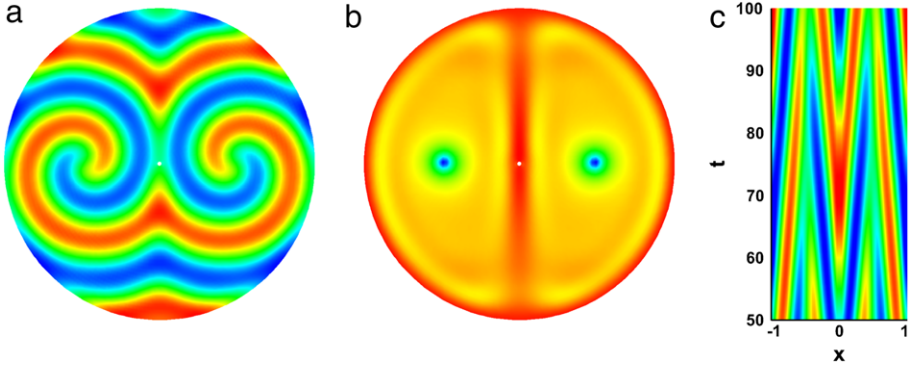


Fig. 5. (Color online) Patterns of (a) $\text{Re}(A)$ and (b) $|A|$ for a pair of stable spiral waves at $t = 50$. (c) is the pattern of $\text{Re}(A)$ at $\theta = 0$ and $\theta = \pi$ denoted by x from $t = 50$ to $t = 100$. Parameters are the same as Fig. 2.

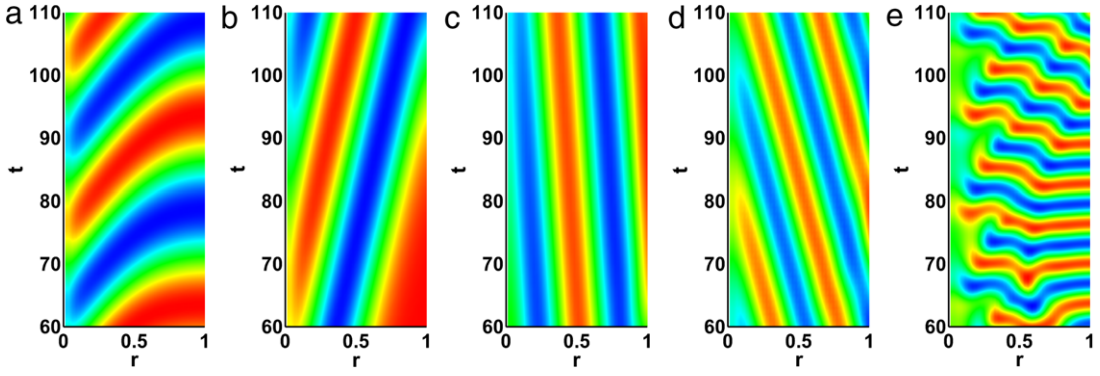


Fig. 6. (Color online) Patterns of $\text{Re}(A)$ at $\theta = 0$ from $t = 60$ to $t = 110$. (a) $d = 1 - 0.2i$ (b) $d = 1$ (c) $d = 1 + 0.2i$ (d) $d = 1 + 0.5i$ (e) $d = 1 + i$. Other parameters are: $\beta = 0.001(1 - 1.35i)$, $a = 1$, lattice size 50×300 , $\Delta r = \Delta\theta = \frac{2\pi}{300}$, $\tau = 1.0$, $c = 100\pi$.

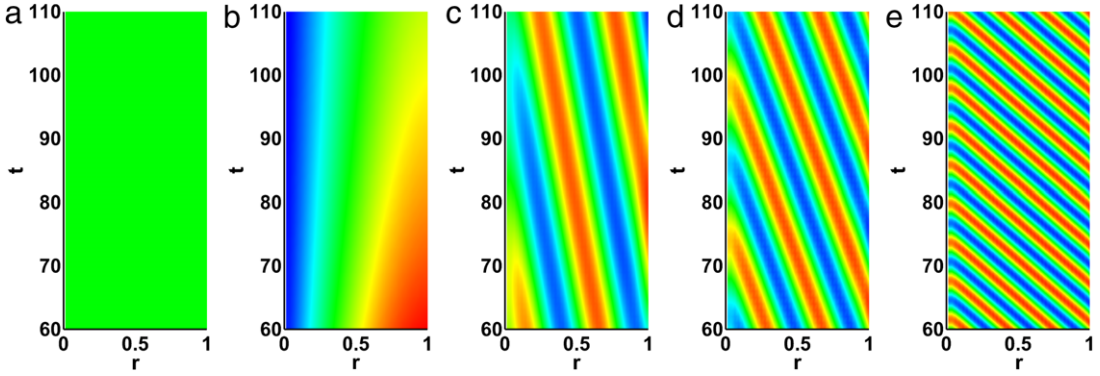


Fig. 7. (Color online) Patterns of $\text{Re}(A)$ at $\theta = 0$ from $t = 60$ to $t = 110$. (a) $a = -1$ (b) $a = 0$ (c) $a = 1$ (d) $a = 2$ (e) $a = 5$. Other parameters are: $\beta = 0.001(1 - 1.35i)$, $d = 1 + 0.34i$, lattice size 50×300 , $\Delta r = \Delta\theta = \frac{2\pi}{300}$, $\tau = 1.0$, $c = 100\pi$.

all the profiles of spiral waves. However, the fifth one is unstable, and will be broken up into spiral turbulence. The patterns show that this parameter can influence the direction of the spiral wave rotating, e.g. (a) and (b) outwardly and (c) and (d) inwardly. Additionally, (a) and (b) show that the region are not filled with the spiral wave at $t = 60$. It means that the velocity of the spiral forming can be influenced by the $\text{Im}(d)$. The wave length is decreasing in this process.

The second test is the linear term coefficient a . We keep the diffusion coefficient $\beta = 0.001(1 - 1.35i)$ and the nonlinear term coefficient $d = 1 + 0.34i$. The patterns of $\text{Re}(A)$ at $\theta = 0$ are shown in Fig. 7. We note that as $a \leq 0$, no spiral wave can be formed, and the maximum value of the region tends to be zero, e.g. 0 in (a) and 0.08 in (b). When $a > 0$, the spiral wave will form. The maximum value of $|A|$ will increase from 1.08, 1.51 to 2.35 as a increased from 1, 2 to 5. The wave length is decreasing in this process.

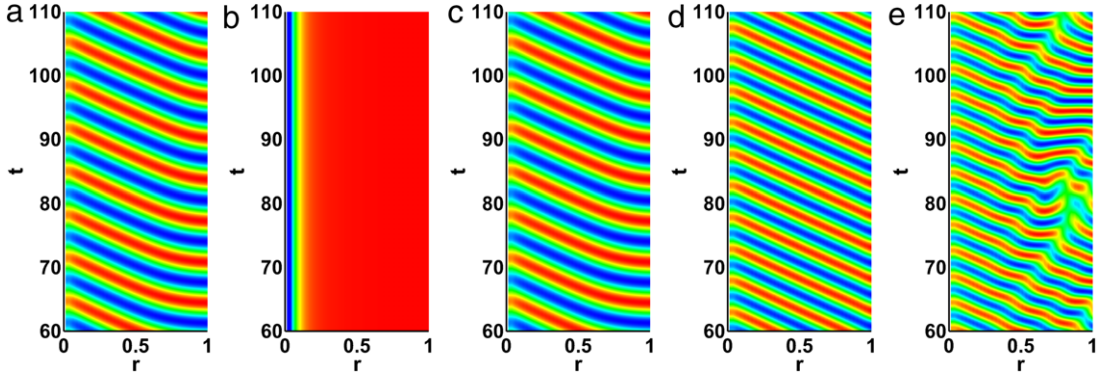


Fig. 8. (Color online) Patterns of $\text{Re}(A)$ at $\theta = 0$ from $t = 60$ to $t = 110$. (a) $d = 1 - i$ (b) $d = 1$ (c) $d = 1 + i$ (d) $d = 1 + 1.5i$ (e) $d = 1 + 2i$. Other parameters are: $\beta = 0.001$, $a = 1$, lattice size 50×300 , $\Delta r = \Delta\theta = \frac{2\pi}{300}$, $\tau = 1.0$, $c = 100\pi$.

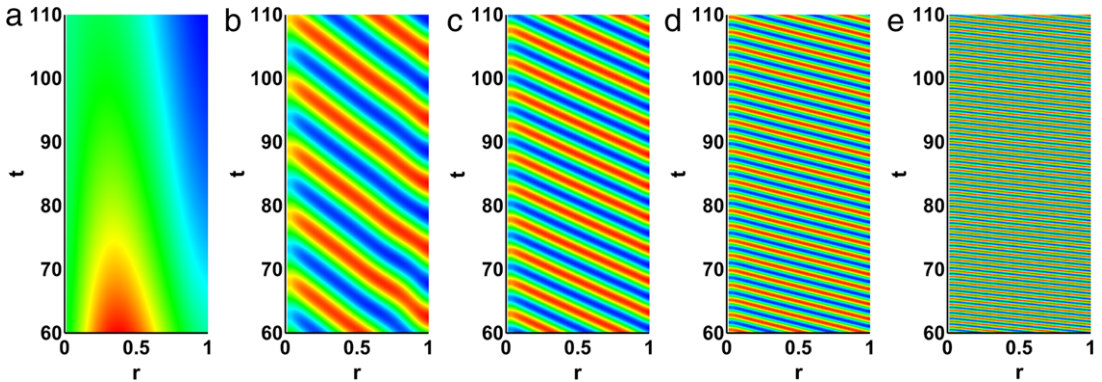


Fig. 9. (Color online) Patterns of $\text{Re}(A)$ at $\theta = 0$ from $t = 60$ to $t = 110$. (a) $a = 0$ (b) $a = 0.5$ (c) $a = 1$ (d) $a = 2$ (e) $a = 5$. Other parameters are: $\beta = 0.001$, $d = 1 + 1.5i$, lattice size 50×300 , $\Delta r = \Delta\theta = \frac{2\pi}{300}$, $\tau = 1.0$, $c = 100\pi$.

The third test is $\text{Im}(d)$ with real diffusion coefficient $\beta = 0.001$ and linear term coefficient $a = 1$. In this case, the value of the $\text{Im}(d)$ is set as $-1, 0, 1, 1.5, 2$, respectively. Fig. 8 shows the pattern of $\text{Re}(A)$ at $\theta = 0$ from $t = 60$ to $t = 110$. We find that when $\text{Im}(d) = 0$, no spiral wave can be formed. The spiral wave will have opposite direction when $\text{Im}(d) = -1$, compared with $\text{Im}(d) = 1$. The wave length is decreasing as $\text{Im}(d)$ increased under the condition $\text{Im}(d) > 0$. $\text{Im}(d) = 2$, the spiral wave is unstable.

If we keep $\beta = 0.001$ and $d = 1 + 1.5i$, we can give the influence of a . As shown in Fig. 9, the spiral wave will form when $a > 0$. As a is increasing, the wave length will be decreased. The maximum value of $|A|$ will satisfy the relation $|A|_{\max} = \sqrt{\text{Re}(a)/\text{Re}(d)}$ [12].

We set $a = 1$, $d = 1 + 1.5i$. The patterns of $\text{Re}(A)$ for different β are given in Fig. 10. In this case, the spiral wave will be formed and rotating inwardly. The wavelength is increasing as $\text{Im}(\beta)$ changes from -0.0001 to 0.001 . From this figure, we can also see that the spiral wave is unstable as $\text{Im}(\beta) \leq -0.0005$. Fig. 11 gives the pattern of $\text{Re}(A)$ for different β with $a = 1$, $d = 1.0 + 0.34i$. When $\text{Im}(d) = 0.34$, the changes of $\text{Im}(\beta)$ will cause the rotating direction changing from outwardly to inwardly, but the wavelength is nearly kept the same.

3.2. Spiral wave on spherical surface

In this section, we demonstrate the advantages of the LBM in spherical coordinates. The initial condition in Eq. (57) is used to simulate spiral waves. We consider the region $0 < \varphi < \pi$, $0 \leq \theta \leq 2\pi$, and lattice size 50×100 . The boundary conditions are the periodic boundary condition for θ , periodic Neumann boundary condition for φ respectively. Because $\varphi = 0$ and $\varphi = \pi$ are two singular points, we select $(\Delta\varphi/2, \Delta\theta/2)$ as a starting point. Fig. 12 shows patterns of $\text{Re}(A)$ and $|A|$ at time $t = 3000$.

This is an unstable initial condition which will create many phase singularities on spherical surface. Under such condition, multi-spiral waves have been observed. And as time goes on, the number of singularities deceases, at last, a frozen state is formed. Fig. 13 shows the multi-spiral waves of $\text{Re}(A)$ with different diffusion coefficient β at time $t = 4000$. These numerical results are similar to the problems on the plane [7], and consistent with our intuition and predictions.

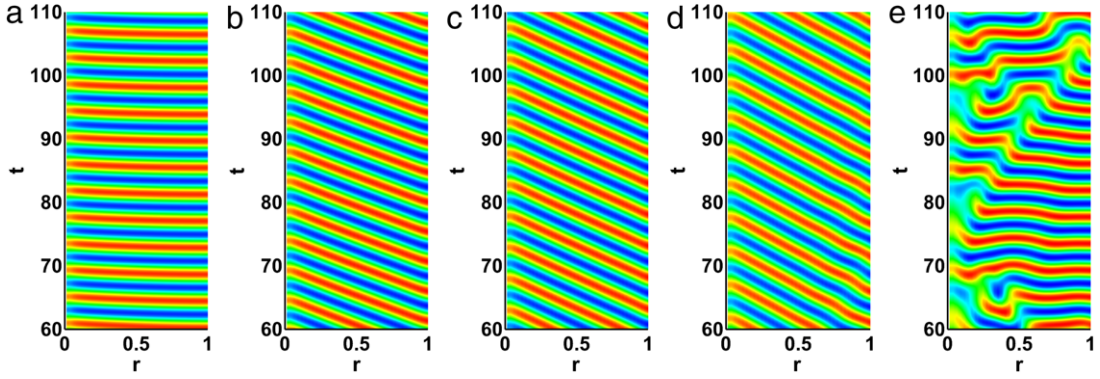


Fig. 10. (Color online) Patterns of $\text{Re}(A)$ at $\theta = 0$ from $t = 60$ to $t = 110$. (a) $\beta = 0.001(1+i)$ (b) $\beta = 0.001(1+0.1i)$ (c) $\beta = 0.001$ (d) $\beta = 0.001(1-0.1i)$ (e) $\beta = 0.001(1-0.5i)$. Other parameters are: $a = 1$, $d = 1 + 1.5i$, lattice size 50×300 , $\Delta r = \Delta\theta = \frac{2\pi}{300}$, $\tau = 1.0$, $c = 100\pi$.

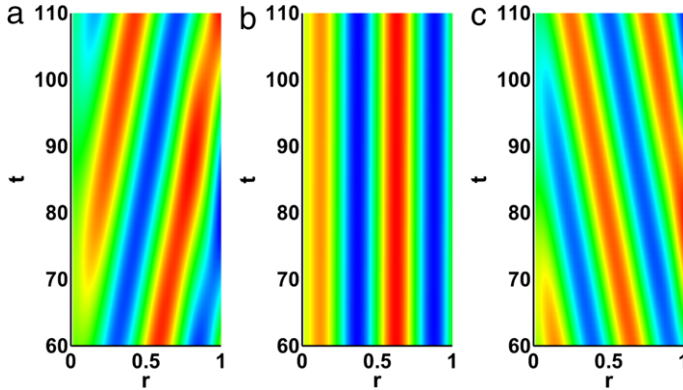


Fig. 11. (Color online) Patterns of $\text{Re}(A)$ at $\theta = 0$ from $t = 60$ to $t = 110$. (a) $\beta = 0.001(1-3i)$ (b) $\beta = 0.001(1-2i)$ (c) $\beta = 0.001(1-1.35i)$. Other parameters are: $a = 1$, $d = 1.0 + 0.34i$, lattice size 50×300 , $\Delta r = \Delta\theta = \frac{2\pi}{300}$, $\tau = 1.0$, $c = 100\pi$.

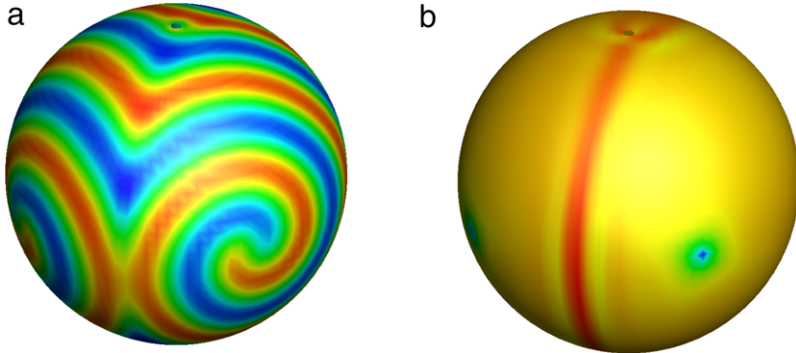


Fig. 12. (Color online) Patterns for stable spiral wave on spherical surface, (a) $\text{Re}(A)$, and (b) $|A|$ at time $t = 3000$. The parameters are: $\beta = 0.001(1-1.35i)$, $a = 1$, $d = 1 + 0.34i$, lattice size 50×100 , $\Delta\varphi = \Delta\theta = 0.02\pi$, $\Delta t = 2.0 \times 10^{-3}$, $c = 10\pi$, $\tau = 1.5$.

3.3. Spiral wave inside ball

Let us consider the 3D region, $0 < \varphi < \pi$, $0 \leq \theta \leq 2\pi$, $0 < r < \pi$, and lattice size $50 \times 100 \times 50$. The boundary conditions are the periodic boundary condition for θ , Neumann boundary condition for r and φ , respectively.

Fig. 14 Shows spiral wave of $\text{Re}(A)$ at different time $t = 0$, $t = 20$, $t = 30$, $t = 40$ by using the LBM in 3D spherical coordinates. The initial value is

$$A(\varphi, \theta, r, 0) = p[r \sin(\varphi) - r_0 + ir \cos(\varphi)]. \quad (59)$$

In Fig. 14(a), the initial value is plotted, where p is $\frac{1}{\pi}$. The spiral wave is induced after $t = 20$ by this unstable ring in Fig. 14(b). From Fig. 14(a)–(d), we display the spiral waves in a sphere which is cut off a quarter. Under such condition,

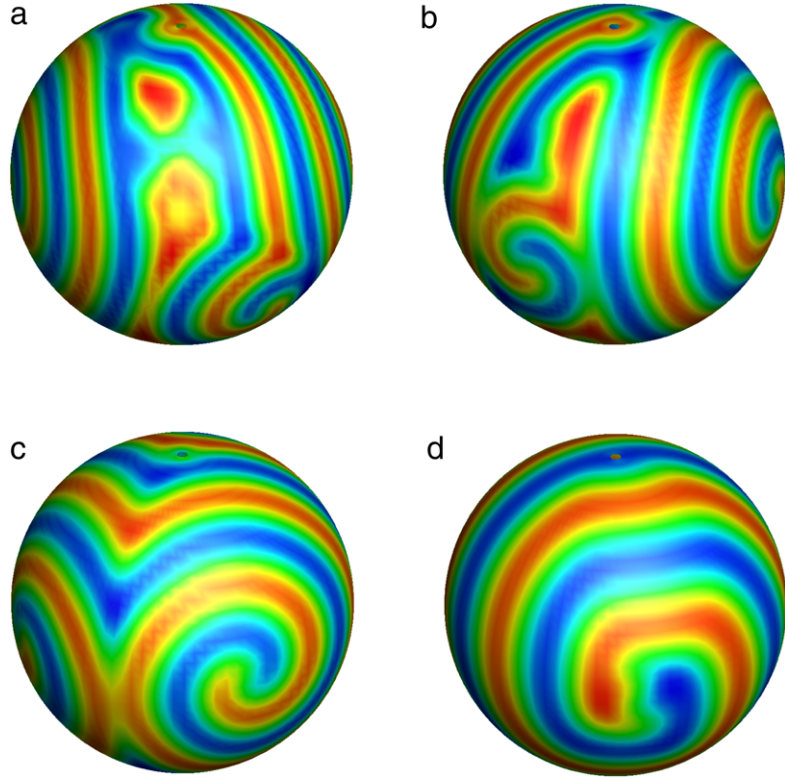


Fig. 13. (Color online) Patterns of $\text{Re}(A)$ for stable spiral wave on spherical surface with different β at time $t = 4000$. (a) $\beta = 0.0005(1 - 1.35i)$ (b) $\beta = 0.0008(1 - 1.35i)$ (c) $\beta = 0.001(1 - 1.35i)$ and (d) $\beta = 0.0015(1 - 1.35i)$. Other parameters are the same as Fig. 12.

multi-spiral waves have been observed; see Fig. 14(c) and (d). These numerical results are similar to the scroll vertex in three dimensional [7], and consistent with our intuition and predictions.

There numerical results that inside ball by LBM are encouraging. It inspires us to further explore the complex spiral structures of the CGLE inside the sphere.

4. Concluding remarks

In conclusion, the spherical coordinate problem is popular when investigating the symmetry of chemical waves, Turing patterns, etc. As a promising numerical method, LBM should be able to deal with the problems in the curvilinear coordinates, such as polar coordinates, spherical surface coordinate, as well as sphere coordinate, which are the motivation and goal of this article.

We can find that the method maintains the algorithmic simplicity of the original lattice Boltzmann scheme, and does not require an interpolation or coarse-graining procedure. This LBM scheme is based on uniformly distributed lattice points in a curvilinear coordinate system. The algorithm provides advantages similar to the lattice Boltzmann method in that it is easily adapted to CGLE.

Different from Cartesian coordinates, the flux term and the source term including φ are emergent due to the curvatures of the coordinates systems. Our philosophy is that the flux is a “pseudo-flux” which has to be treated as a source term, rather than a flux term. Examples show that the model accurately reproduces the phenomena in the CGLE.

There are many other systems where patterns form on the spherical surface and insider sphere in nature [13]. The bimolecular autocatalytic reaction-diffusion systems such as Fitzhugh-Nagumo system, Gray-Scott system, Belousov-Zhabotinsky system etc, also need to simulate.

We believe that our results constitute a first step toward the exploration for more complex model in non-Euclidean spaces by lattice Boltzmann method. The approach, those “pseudo-flux” due to the curved surface, as well as the structure of the equilibrium distribution functions, is the enlightenment for simulating other similar systems.

It should be noted that the lattice Boltzmann model for Navier-Stokes equations and magnetohydrodynamics on sphere should be paid attention to since their difficulties. We have also explored the LBM with sphere coordinate, and tentatively simulate some of the problems within a sphere. But we find that the radial “pseudo-flux” will also occur, which causes the problem even more troublesome. Above problems are our interests.

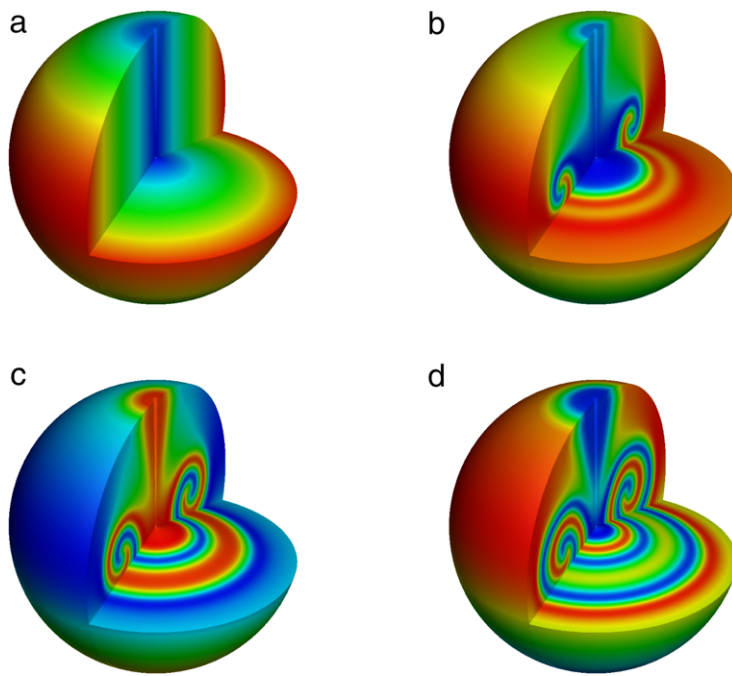


Fig. 14. (Color online) The spiral waves of $\text{Re}(A)$ in 3D spherical coordinate at different time (a) $t = 0$ (b) $t = 20$ (c) $t = 30$ (d) $t = 40$. The parameters are: $\beta = 0.002(1 - 1.35i)$, $a = 1$, $d = 1 + 0.34i$, $r_0 = 0.5$, lattice size $50 \times 100 \times 50$, $\Delta\varphi = \Delta r = \Delta\theta = 0.02\pi$, $c = 10\pi$, $\tau = 1.5$.

References

- [1] S.Y. Chen, G.D. Doolen, Lattice Boltzmann method for fluid flows, *Annu. Fluid Mech.* 3 (1998) 314–322;
C.K. Aidun, J.R. Clausen, Lattice-Boltzmann method for complex flows, *Annu. Rev. Fluid Mech.* 42 (2010) 439–472.
- [2] S. Succi, *The Lattice Boltzmann Equation for Fluid Dynamics and Beyond*, Oxford University Press, New York, 2001.
- [3] S.Y. Chen, H.D. Chen, D. Martinez, et al., Lattice Boltzmann model for simulation of magnetohydrodynamics, *Phys. Rev. Lett.* 67 (1991) 3776–3779.
- [4] S. Succi, Numerical solution of the Schrödinger equation using discrete kinetic theory, *Phys. Rev. E* 53 (1996) 1969–1975.
- [5] J. Yepez, B. Boghosian, An efficient and accurate quantum lattice- gas model for the many- body Schrödinger wave equation, *Comput. Phys. Comm.* 146 (2002) 280–294.
- [6] S. Palpacelli, S. Succi, R. Spigler, Ground- state computation of Bose- Einstein condensates by an imaginary- time quantum lattice Boltzmann scheme, *Phys. Rev. E* 76 (2007) 036712;
S. Palpacelli, S. Succi, Quantum lattice Boltzmann simulation of expanding Bose- Einstein condensates in random potentials, *Phys. Rev. E* 77 (2008) 066708.
- [7] J.Y. Zhang, G.W. Yan, Lattice Boltzmann model for the complex Ginzburg- Landau equation, *Phys. Rev. E* 81 (2010) 066705;
J.Y. Zhang, G.W. Yan, Numerical studies based on higher-order accuracy lattice Boltzmann model for the complex Ginzburg- Landau equation, *J. Sci. Comput.* 52 (2012) 656–674;
J.Y. Zhang, G.W. Yan, Three-dimensional lattice Boltzmann model for the complex Ginzburg- Landau equation, *J. Sci. Comput.* 60 (2014) 660–683.
- [8] J.Y. Zhang, G.W. Yan, Lattice Boltzmann model for the bimolecular autocatalytic reaction- diffusion equation, *Appl. Math. Model.* 38 (2014) 5796–5810.
- [9] X.Y. He, G.D. Doolen, Lattice Boltzmann method on a curvilinear coordinate system: Vortex shedding behind a circular cylinder, *Phys. Rev. E* 56 (1997) 434–440.
- [10] M. Bouzidi, D. d'Humieres, P. Lallemand, L.-S. Luo, Lattice Boltzmann equation on a two-dimensional rectangular grid, *J. Comput. Phys.* 172 (2001) 704–717;
R.G.M. van der Sman, H. Ernst, Convection- diffusion lattice Boltzmann scheme for irregular lattices, *J. Comput. Phys.* 160 (2000) 766–782.
- [11] H. Yoshida, M. Nagaoka, Lattice Boltzmann method for the convection- diffusion equation in curvilinear coordinate systems, *J. Comput. Phys.* 257 (2014) 884–900.
- [12] J.R. Weimar, J.P. Boon, Class of cellular automata for reaction- diffusion systems, *Phys. Rev. E* 49 (1994) 1749–1752.
- [13] C. Varea, J.L. Arago'n, R.A. Barrio, Turing patterns on a sphere, *Phys. Rev. E* 60 (1999) 4588–4592;
S. Bhattacharya, Galerkin model for Turing patterns on a sphere, *Phys. Rev. E* 72 (2005) 036208.